International Forum on Aeroelasticity and Structural Dynamics
IFASD 2024
17-21 June 2024, The Hague, The Netherlands

NONLINEAR AEROELASTIC RESPONSE ANALYSIS OF UNMANNED MULTI-BODY AIRCRAFT WITH FREE PLAY

Zhu Chen[1, 2, 3, 4], Bi Ying[1, *], Zhu Zijian[1], Ying Zhuolin[1], Ma Xiaoping[1]

[1, *] Institute of Engineering Thermophysics, Chinese Academy of Sciences, Beijing, 100190, China;

[2] School of Aeronautics and Astronautics, University of Chinese Academy of Sciences, Beijing, 100049, China;

[3] National Key Laboratory of Science and Technology on Advanced Light-Duty Gas-Turbine, Beijing, 100049, China;

[4] Key Laboratory of UAV Emergency, Rescue Technology, Ministry of Emergency Management, Beijing, 102202, China

Keywords: Aeroelastic Analysis, Unmanned Multi-body Aircraft, Free Play

Abstract: For the unmanned multi-body aircraft (MBA), free plays are commonly found at the flexible hinges between adjacent flight units, and its nonlinear characteristics will result in the deviation of aircraft aeroelastic stability boundary, so it is necessary to carry out the research that takes into account the free-play nonlinearity in the context of aeroelastic response analysis. The research focuses on the free play in the rotation direction at the wingtip of an unmanned multi-body aircraft. Based on the fictitious mass method, an appropriate fictitious mass is selected at a suitable position, and the modal shape is linearized to establish a unified modal array capable of expressing deformations across the entire response spectrum. Besides, rational function fitting is used to convert the unsteady aerodynamic forces in the frequency domain to the time domain, and the limit cycle response characteristics corresponding to different free-play parameters are analyzed. The results show that when there is a free play between the wings of an unmanned multi-body aircraft, nonlinear limit cycle oscillations occur within a specific region below the linear flutter threshold, and the parameters defining these free plays have a notable impact on the amplitude of these limit cycle oscillations and the speed at which divergence occurs.

1 INTRODUCTION

In recent years, high-altitude long-endurance unmanned aerial vehicles (HALE UAVs) have been increasingly used in military and civilian aviation industries[1,2]. In order to meet the requirements of long endurance, high aspect ratio wings are widely adopted. However, while the high aspect ratio configuration brings better aerodynamic characteristics to the UAVs, it also imposes more stringent requirements for their takeoff and landing environments, transportation conditions, and structural strengths, especially in the relatively harsh flight environments at low altitudes where atmospheric turbulence makes its aeroelastic stability and response issues more prominent[3,4]. Consequently, the unmanned multi-body aircraft has emerged.

The unmanned multi-body aircraft (MBA) represents a novel aircraft configuration combining multiple fixed-wing UAVs through various connection methods. It adopts the method of independent takeoff and landing of several individual units followed by assembly in the air, which can effectively address the issues of poor wind resistance, difficult low-altitude flight, poor mission maneuverability, low battlefield survivability, and high system health requirements associated with high aspect ratio aircraft. Additionally, it breaks through the limitations of traditional aspect ratio designs, allowing for a greater overall lift-to-drag ratio of the aircraft.

The concept of the unmanned MBA can be traced back as far as the 1940s when Dr.Vogt proposed the wingtip docking idea, which was accomplished by a rope passing through the wingtips and a winch on the aircraft[5]. In the following half century, several countries conducted similar experiments. However, due to the imperfection of theoretical systems and the absence of technical aspects, none of the experiments achieved the desired results[6,7]. With the continuous exploration of the near-space in recent years, the unmanned MBA has regained the attention of the aeronautical community. Magill et al.[8] found that the wingtip docking method of the unmanned MBA increased the total system span and can gain 20% to 40% improvement in range performance. Wlach et al.[9] reconfigured the aircraft using a highly resilient wing and a segmented aircraft approach, proposing an unmanned MBA configuration that takes elasticity into account. Montalvo et al.[10] introduced the concept of meta aircraft, achieving docking at the wingtips through magnetic connections. Subsequently, Montalvo's team conducted further research on the flight dynamics, control, and stability of meta aircraft, which also verified the controllability and feasibility of the wingtip connection configuration[11,12]. Meng et al.[13] proposed the use of a hinged structure for wingtip docking of the aircraft, which allows only relative roll motion between two aircraft. Alexander's team also conducted separate studies on flight dynamics, dynamical processes of the connection behaviour and controllability for this configuration, and the result shows that this solution has good feasibility[14,15].

From the above, it can be seen that the research on the unmanned MBA has primarily focuses on the feasibility analysis and the dynamics analysis of the docking process, with relatively little research conducted on aeroelastic characteristics, which is often limited to linear studies. However, there are structural gaps at the docking areas between adjacent flight units, which lead to certain nonlinear characteristics of the stiffness. This can cause deviations in the aeroelastic stability boundaries of the aircraft, affecting the aircraft's handling stability characteristics and flight quality. Therefore, it is necessary to carry out the research on the aeroelastic response analysis of the unmanned MBA that considers the nonlinearity of free plays.

Plenty of research works have been carried out on nonlinear aeroelastic analysis for free plays, and the methods mainly includes the equivalent linearization method[16,17], harmonic balance method[18], numerical integration method[19,20], dynamic substructure method[21], and fictitious mass method[22]. Among them, Zhang Weiwei[23] used the equivalent linearization method to analyze the flutter characteristics of the rudder surface with nonlinear free plays. Lee et al.[24] used the harmonic balance method to study the nonlinearity of a binary airfoil segment. Yang et al.[25] established a nonlinear dynamics modelling method based on the dual-coordinated free-interface dynamic substructures method for multi-degree-of-freedom engineered structures, carried out a folded wing nonlinear response analysis and compared with the wind tunnel test results. Li Jiaxu[26] obtained the nonlinear aeroelastic equations through the Lagrange equation for the control rudder structural model, and investigated the effects of free plays in pitch and

plunge directions respectively. Zhang Fei[27] conducted nonlinear flutter analysis of the manoeuvring surface gaps using a time-domain method and compared it with the frequency description equation technique. Wang Fei[22] used the fictitious mass method for nonlinear aeroelastic response analysis of the fully moving wing with free play, and designed a set of rapid analysis methods while meeting the basic requirements of engineering design.

Above all, most research for nonlinear aeroelastic analysis with free play has mainly focused on analytical methods and nonlinear effects, and most of the research objects are two-dimensional low-speed model of single UAV rudder surface. In this paper, a nonlinear aeroelastic response analysis is carried out for a two-aircraft combined unmanned multi-body aircraft with wingtip hinge connections. Then, fictitious mass method are used to linearising the modal shape, and the rational function fitting is used to convert the unsteady aerodynamic forces in the frequency domain to the time domain to solve the corresponding aeroelastic issues. Moreover, the study separately investigates the effects of the parameters defining the free plays like gap values, gap stiffness characteristics, and damp coefficients on structural nonlinearities, with the hope of providing references for the design of wingtip docking for the unmanned multi-body aircraft.

2 THEORY

2.1 Nonlinear Aeroelastic Equation with Free Play

Aeroelastic equations are a set of equations describing the dynamic response of a vehicle during flight due to the interaction between aerodynamic forces and structural elastic deformation. In practical engineering applications, these equations are often very complex and difficult to solve directly. In order to simplify the problem and improve analysis efficiency, they are typically transformed into modal space for solution. The nonlinear aeroelastic equations with free play can be represented as

$$\Phi^T M \Phi \ddot{q} + \Phi^T C \Phi \dot{q} + \Phi^T K \Phi q = q_\infty \Phi^T A \Phi q \tag{1}$$

Where M is the structural mass matrix, kg; C is the structural damping matrix, kg/s; K is the structural stiffness matrix, N/m; Φ is the modal matrix, dimensionless; q is the generalized modal coordinate vector, m; q_∞ is the dynamic pressure, Pa; A is the aerodynamic influence coefficient matrix, m.

Without considering the large geometric deformations, the nonlinearity of free play is mainly reflected in the stiffness matrix K and the modal matrix Φ in the aeroelastic equations.

2.2 Fictitious Mass Method

Due to the existence of two nonlinear terms K and Φ in the nonlinear aeroelastic equations with free play, the fictitious mass method is used to linearize the modal shape to reduce the difficulty of solving the equations. The basic idea of the fictitious mass method is to establish a unified modal array capable of expressing deformations across the entire response spectrum, ensuring the continuous deformation of the structure during the time-domain integration process [28,29].

The fictitious mass method is implemented by applying a concentrated mass ΔM to the original structural model without considering the free play, thereby establishing a modal shape that

includes fictitious mass. The position of the applied fictitious mass is generally chosen near the structural gap. Neglecting the damping term, the free vibration equation of the structure after applying the fictitious mass can be expressed as

$$[-\omega_{FM}{}^2(M+\Delta M)+K_1]\Phi_{FM}=0 \tag{2}$$

Where ΔM is the fictitious mass, kg; Φ_{FM} is the modal matrix with fictitious mass, dimensionless; ω_{FM} is the modal frequency with fictitious mass, rad/s; K_1 is the stiffness matrix of the structure without free play, N/m.

Subsequently, the nonlinear modal shapes in the nonlinear aeroelastic equation are replaced using modal shapes with fictitious mass, while the fictitious mass is removed and the structural mass matrix, damping matrix, stiffness matrix, and aerodynamic influence coefficients matrix are generalized, from which Eq.(1) can be expressed as

$$\Phi_{FM}{}^T M\Phi_{FM}\ddot{q}+\Phi_{FM}{}^T C\Phi_{FM}\dot{q}+\Phi_{FM}{}^T K\Phi_{FM}q=q_\infty\Phi_{FM}{}^T A\Phi_{FM}q \tag{3}$$

From Eq.(3), it can be seen that at this point, the nonlinear term in the nonlinear equation with free play only includes the structural stiffness matrix K.

2.3 Rational Function Fitting

In engineering applications, the doublet lattice method is often used to solve for unsteady aerodynamic forces. This method is a panel method based on the harmonic oscillation assumption and the frequency domain equation of the small perturbation velocity potential. Since nonlinear aeroelastic analysis with free play generally requires the unsteady aerodynamic forces for arbitrary system motion in the time domain, this paper proposes to uses the Minimal State (MS) approximation to transform the aerodynamic data in the frequency domain into the time domain. Specifically, it utilizes the unsteady aerodynamic forces corresponding to several discrete frequency points, extends them into the Laplace domain, and expresses them with rational functions. By fitting the rational functions, the unknown coefficients are obtained. Then, aerodynamic force state variables are introduced, the time-domain differential equations satisfied by the aerodynamic state variables are further obtained, and finally the entire aeroelasticity equations are expressed in the state-space form.

The minimum state method involves approximating the aerodynamic influence matrix Q in the Laplace domain as follows

$$Q\approx A_0+A_1\bar{s}+A_2\bar{s}^2+D(\bar{s}I-R)^{-1}E\bar{s} \tag{4}$$

Where Q is the aerodynamic force matrix, m; A_0, A_1, A_2, D, E are the matrices of undetermined coefficients, which can be solved iteratively using ordinary least squares; R is the aerodynamic lag matrix; $\bar{s}=sb/V$ is the dimensionless Laplace variable.

2.4 State-Space Equations for Nonlinear Structures with Free Play

The wingtip hinge docking part of the unmanned multi-body aircraft has a free play in the rotation direction, so this paper takes the bilinear free play as the research object and simulates the nonlinear stiffness of free play with a linear spring. The system stiffness is a nonlinear parameter that varies with the response displacement. When the absolute value of the model displacement is less than the gap value b , the stiffness of the linear spring is 0; when the absolute value of the model displacement is greater than or equal to the gap value b , the stiffness of the linear spring is K_0, as shown in Figure 1.

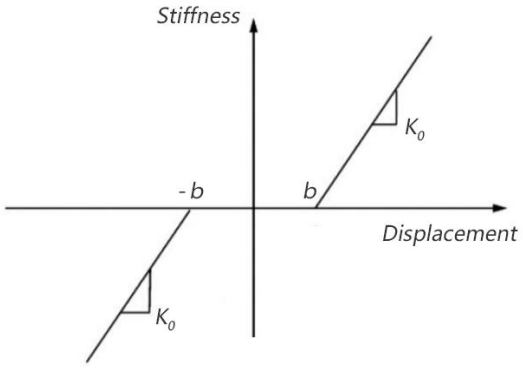

Figure 1 Diagram of nonlinear stiffness of free play

According to the nonlinear characteristic curve of free play shown in Figure 1, the nonlinear system could be decomposed into three linear subsystems corresponding to each segment of the curve shown in Figure 1, and neglecting the damping term, the control equations could be respectively expressed as

$$\begin{cases} \overline{M_{norm}}\ddot{q} + \overline{K_{norm}}q = q_\infty \overline{Q}q, & d \geq +b \\ \overline{M_{norm}}\ddot{q} + \overline{K_{free}}q = q_\infty \overline{Q}q, & -b < d < b \\ \overline{M_{norm}}\ddot{q} + \overline{K_{norm}}q = q_\infty \overline{Q}q, & d \leq -b \end{cases} \tag{5}$$

Where $-b < d < b$ is the range of free play, with d being the response displacement and b the gap value; $\overline{M_{norm}} = \Phi_{FM}{}^T M \Phi_{FM}$ is the generalized structural mass matrix; $\overline{K_{norm}} = \Phi_{FM}{}^T K_{norm} \Phi_{FM}$ is the generalized stiffness matrix of the Nominal Structure excluding the free play section $|d| \geq b$; $\overline{K_{free}} = \Phi_{FM}{}^T K_{free} \Phi_{FM}$ is the generalized stiffness matrix of the Freeplay Structure, which is typically obtained by setting the stiffness of the linear spring at the wingtip hinge docking part of the unmanned MBA system to 0; $\overline{Q} = \Phi_{FM}{}^T A \Phi_{FM}$ is the generalized aerodynamic force matrix.

Write the equations of motion for each linear system in Eq.(5) in a unified form, and get

$$M_{hh}(V_1, V_2, \ldots V_n)\ddot{q} + K_{hh}(V_1, V_2, \ldots V_n)q = Q_{hh}(V_1, V_2, \ldots V_n)q \tag{6}$$

Where M_{hh}, K_{hh} are the generalized mass matrix and the generalized stiffness matrix; Q_{hh} is the unsteady aerodynamic force matrix; $V_i, i = V_1, V_2, ...V_n$ is the nonlinear parameter, with n being the number of values the nonlinear parameter can take. Assuming there are m groups of nonlinear parameters, with each group having n values, then the total number of nonlinear parameters is $m \times n$, and each nonlinear parameter V_{ij} will generate $m \times n$ coefficient matrices. Within each nonlinear parameter V_{ij}, the aeroelastic system is locally linear, that is, $M_{hhij}, K_{hhij}, Q_{hhij}$ are constant, resulting in $m \times n$ sets of state-space equations.

$$\left\{\dot{X}_{ae}\right\} = \left[A_{ae}\right]_{ij} \left\{X_{ae}\right\} + \left[B_{ae}\right]_{ij} \left\{u_{ae}\right\} \tag{7}$$

Where X_{ae} includes the matrices for structural and aerodynamic states, u_{ae} represents external disturbances. The time-domain state-space equation in discrete-time propulsion format is represented as

$$\left\{X\right\}_{k+1} = \left[\overline{A}\right]_{ij} \left\{X\right\}_k + \left[\overline{B}\right]_{ij} \left\{u\right\}_k \tag{8}$$

Where k is a time incremental index.

2.5 Analysis Process

In the traditional aeroelastic response analysis process, modal analysis must be conducted first, followed by aeroelastic analysis based on that. This process must be repeated for each set of structural parameters. The method presented in this paper involves applying concentrated mass at appropriate positions on the original structure model without free play, conducting modal analysis to obtain the fictitious mass modal shape. And then this modal shape is used to replace the modal shape of the nonlinear system, and using this modal as a fixed unified modal. The position for applying the fictitious mass is generally chosen to be close to the target parameter research area, without generating low-frequency local modes, and the size is essentially in a same order of magnitude with the total mass of the model.

When structural parameters are locally changed, modal analysis is no longer carried out; instead, the fictitious mass modal shape is directly utilized to generalize the mass matrix, damping matrix, stiffness matrix, and aerodynamic force matrix under different model parameters, and then solve the aeroelastic equations. The response of the nonlinear system divides the nonlinear system into several linear subsystems, and the nonlinear equations of the unmanned MBA with free play are solved using the discrete-time state-space method.

First, a discrete locally linear state space coefficient matrices $\left[\overline{A}\right]_{ij}$ and $\left[\overline{B}\right]_{ij}$ is constructed on each discrete nonlinear parameter. Then, during the process of time-domain integration and solution, within each time step, the nonlinear parameters V_{ij} are first calculated, and then based on the $m \times n$ discrete state spaces $\left[\overline{A}\right]_{ij}$ and $\left[\overline{B}\right]_{ij}$, the state-space matrices $\left[A\right]$ and $\left[B\right]$ of the current time step are constructed using interpolation methods, and the updated state-space

matrices $[A]$ and $[B]$ are used to calculate the transient response results for the next time step. The specific solution steps are shown in Figure 2.

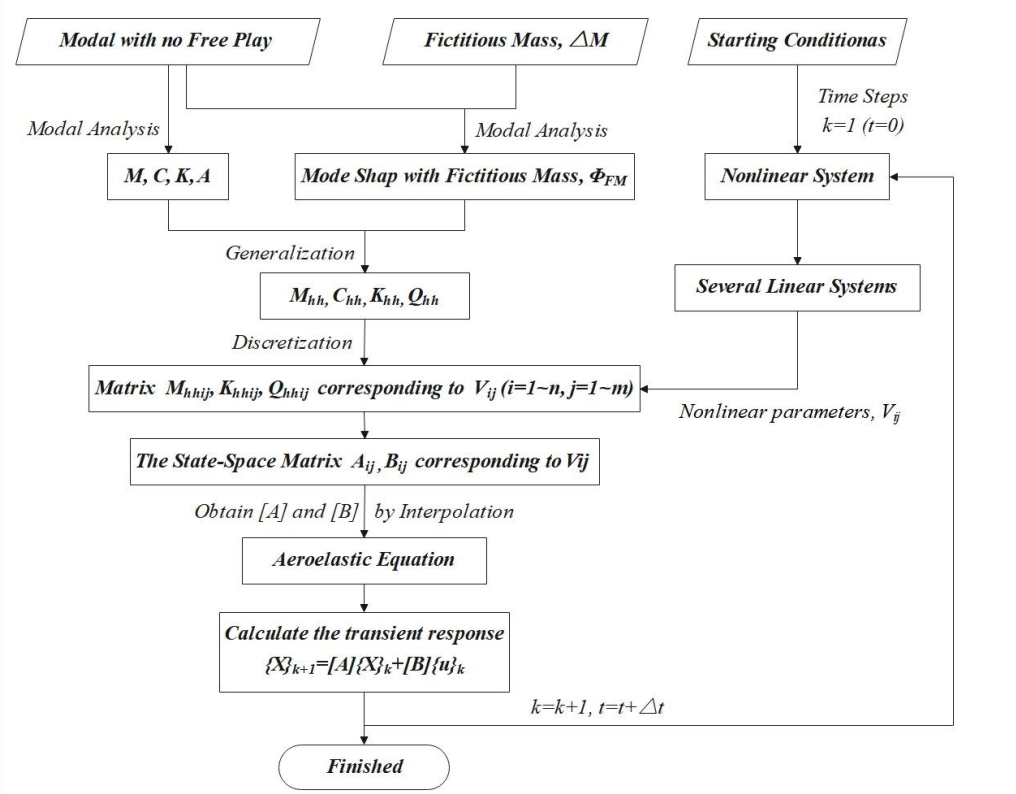

Figure 2 Analysis flow chart

3 EXAMPLE AND ANALYSIS

3.1 Basic Parameters

In this paper, a flexible wing model with high aspect ratio is used to illustrate the nonlinear effect of free play on the aeroelastic stability of the unmanned multi-body aircraft. The schematic diagram of the wing structure of the single unmanned MBA is shown in Figure 3, the aircraft has a wingspan of 2 m and a chord length of 0.1 m. The airfoil has a single girder structure, with the main spar made of steel, the ribs made of aluminum, and the space between the girders filled with rigid foam. The basic parameters are described in Table 1.

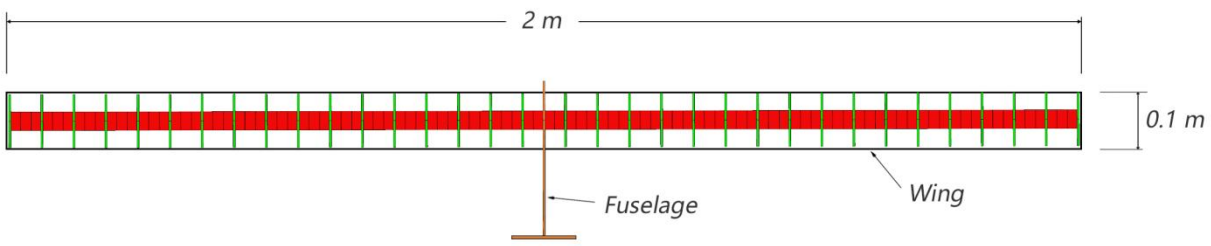

Figure 3 Sketch map of wing parameters of the single unmanned MBA

Table 1 Modal parameters of unmanned MBA

Parameters	Values	Parameters	Values
Span Length/m	2.000	Position of Main Beam	50% Chord Length
Chord Length/m	0.100	Modulus of Elasticity of Main Beam/GPa	395.1
Structural mass/kg	1.215	Cross-section Size of Main Beam/m	0.035×0.0015

This article focuses on a two-aircraft combined unmanned multi-body aircraft with wingtip hinge connections, taking the bilinear free play as the research object and conducting a nonlinear aeroelastic analysis of the free play. For the treatment of the nonlinear system, this article uses spring elements for simulation. The two UAVs are constrained by the RBE2 joint in three translational degrees of freedom and rotations around the y-axis and z-axis, and the rotational degrees of freedom around the rotary axis are constrained by the CELAS1 spring element. The schematic diagram after the two UAVs are connected is shown in Figure 4-5, with a gap of 0.005m between them. The hinge structure between them contains a spindle and a normal spring of the wing surface, where the spindle provides bending stiffness, and the normal spring of the wing surface provides rotational stiffness. It is assumed that the model has a free play in the rotation direction, and the nonlinear stiffness of the free play is simulated by this spring element.

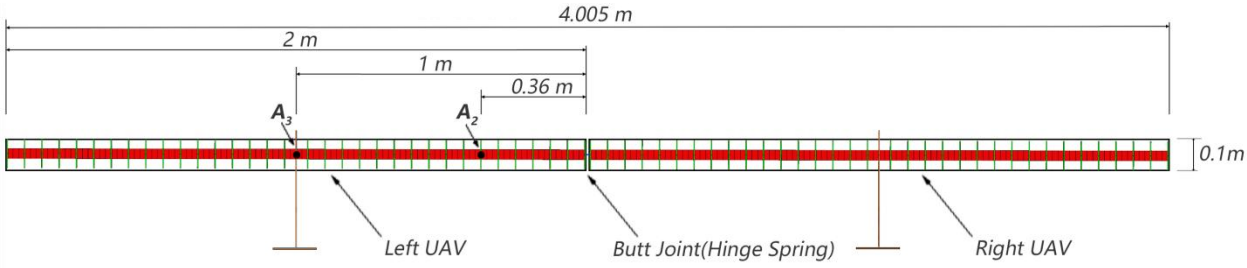

Figure 4 The schematic diagram of a two-aircraft combined unmanned MBA

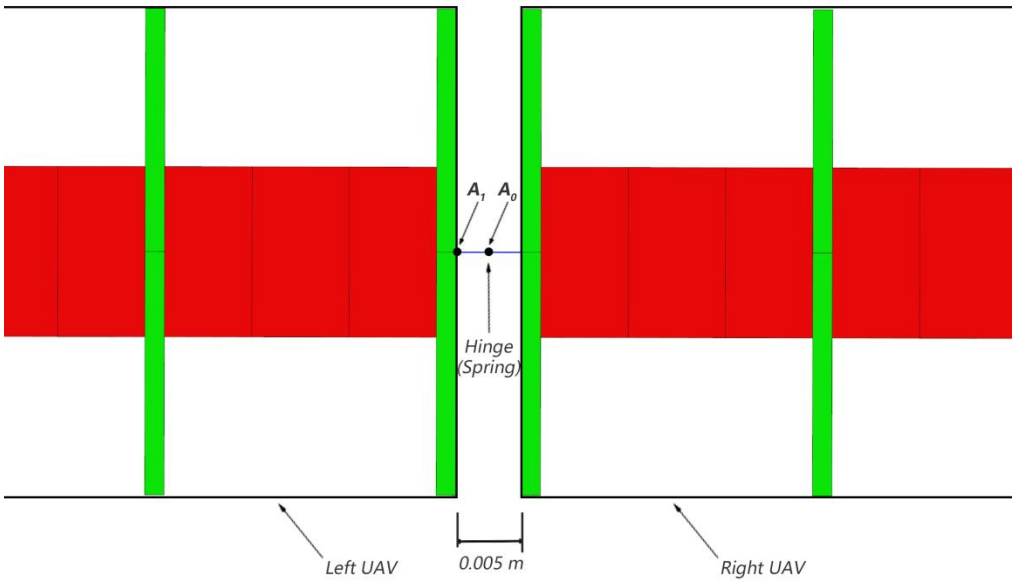

Figure 5 Detailed view of the docking area of a two-aircraft combined unmanned MBA

3.2 Set up of the Fictitious Mass

The nonlinear system is modeled by the fictitious mass method, which produces fictitious mass modal shape by applying a fictitious mass to the free play area of the original structure, and then this fictitious mass is removed from the generalized mass matrix to prevent the construction of the state-space equations from affecting the dynamical characteristics of the original structure. The fictitious mass is simulated using finite element concentrated mass elements during implementation. In order to investigate the effects of the magnitude and position of the fictitious mass on the analysis results, this paper selects 8 configurations of fictitious mass as shown in Table 2. Among them, $\Phi_1 \sim \Phi_3$ corresponding to points A_0, $\Phi_4 \sim \Phi_6$ corresponding to points A_1, Φ_7 corresponding to points A_2, Φ_8 corresponding to points A_3. The application positions of each point are shown in Figure 4-5, while A_0 is located at the centre of the docking interval between the two aircraft, A_1 is located on the wingtip beam element of the single UAV on one side of the docking, A_2 is located on the beam element approximately one-third of the semi-span away from the wingtip of the single UAV, and A_3 is located on the beam element where the center of gravity of the single UAV is situated. Using the modal shape corresponding to these 8 fictitious masses, based on the frequency-domain method, vibration and flutter analysis are carried out for the target model without fictitious mass applied with linear spring stiffness of 0 and 2000 N/mm, respectively, and compared with the results of the direct calculations, as shown in Table 3-4. From the results, it can be seen that the calculation result corresponding to Φ_5 has the smallest error, and part of the modal shape is shown in Figure 6. The subsequent analyses will proceed using this fictitious mass, with its application position at A_1 and a magnitude of 1 kg, indicating that the size of the fictitious mass is on the same order of magnitude as the model.

Table 2 Set up of modal shape with different fictitious mass

Modal Shape	Fictitious Mass Application Position	Fictitious Mass Size / kg
Φ_0	/	/
Φ_1	A_0	0.1
Φ_2	A_0	1.0
Φ_3	A_0	10.0
Φ_4	A_1	0.1
Φ_5	A_1	1.0
Φ_6	A_1	10.0
Φ_7	A_2	1.0
Φ_8	A_3	1.0

Table 3 Calculation results with different fictitious mass modal shape at $K = 0N/mm$

Modal Shape	Anti-symmetric 1st bend frequency / Hz	Symmetric 2nd bend frequency / Hz	In-plane symmetric 1st bend frequency / Hz	1st torsion frequency / Hz	In-plane anti-symmetric 1st bend frequency / Hz	Flutter speed / m/s
Φ_0	1.539	2.216	13.07	22.91	35.87	18.00
Φ_1	1.539	2.075	12.70	22.91	35.87	11.33
Φ_2	1.539	1.724	10.91	22.91	35.87	15.95
Φ_3	1.539	1.563	8.772	22.91	35.87	19.91
Φ_4	1.539	2.076	12.70	22.91	35.87	15.33
Φ_5	1.539	1.728	10.91	22.91	35.87	18.44
Φ_6	1.539	1.567	8.772	22.91	35.87	22.67
Φ_7	1.417	2.193	11.47	22.91	33.08	22.05
Φ_8	1.296	2.022	13.00	22.91	30.74	24.11

Table 4 Calculation results with different fictitious mass modal shape at $K = 2000N/mm$

Modal Shape	Anti-symmetric 1st bend frequency / Hz	Symmetric 2nd bend frequency / Hz	In-plane symmetric 1st bend frequency / Hz	1st torsion frequency / Hz	In-plane anti-symmetric 1st bend frequency / Hz	Flutter speed / m/s
Φ_0	1.539	2.485	13.07	22.91	35.87	24.00
Φ_1	1.539	2.338	12.70	22.91	35.87	24.10
Φ_2	1.539	1.928	10.91	22.91	35.87	24.09
Φ_3	1.539	1.723	8.772	22.91	35.87	22.00
Φ_4	1.539	2.485	13.07	22.91	35.87	24.09
Φ_5	1.539	2.339	12.70	22.91	35.87	24.00
Φ_6	1.539	1.932	10.91	22.91	35.87	24.19
Φ_7	1.417	2.193	11.47	22.91	33.08	22.16
Φ_8	1.296	2.022	13.00	22.91	30.74	22.25

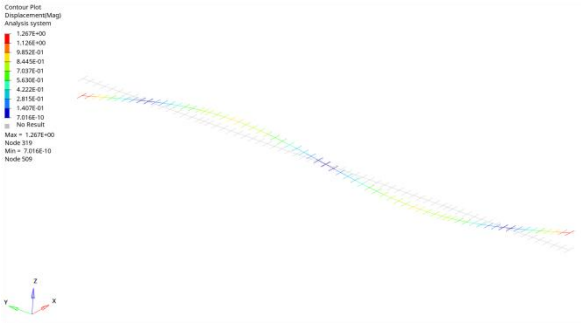

(a) Anti-symmetric 1st bending mode

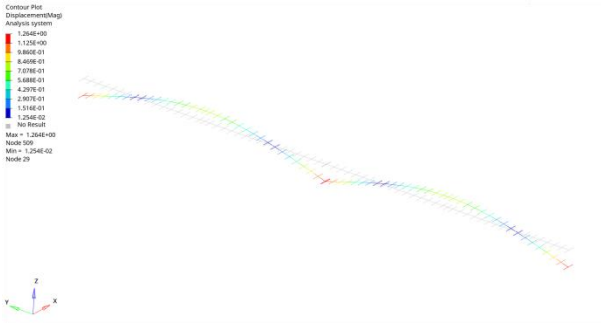

(b) Symmetric 2nd bending mode

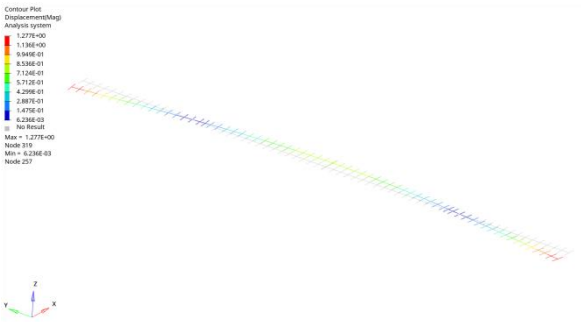

(c) In-plane symmetric 1st bending mode

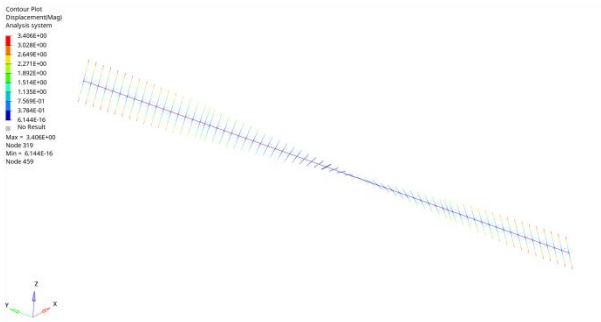

(d) 1st torsion mode

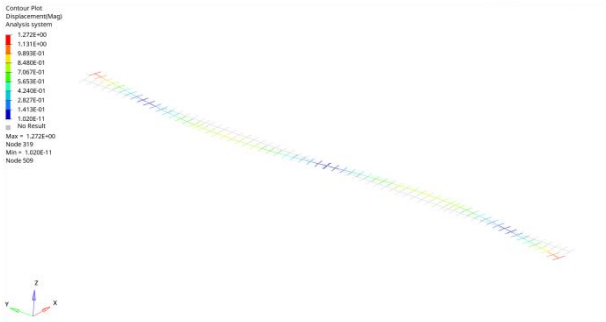

(e) In-plane anti-symmetric 1st bending mode

Figure 6 Typical modal shape considering fictitious mass

3.3 Nonlinear Transient Response Analysis with Free Play

In order to compare with the results of the nonlinear analysis of free play, the time-domain linear transient response analysis are conducted for the case where the gap value b is 0 mm and the stiffness K_0 is 2000 N/mm. The vertical displacement of the center of the wingtip of a single aircraft is measured, and the results are shown in Figure 7. It can be observed that there is a clear boundary in the linear time-domain response analysis results, when the speed is below 24.00 m/s, the response converges; when the speed is above or equal to 24.00 m/s, the response diverges.

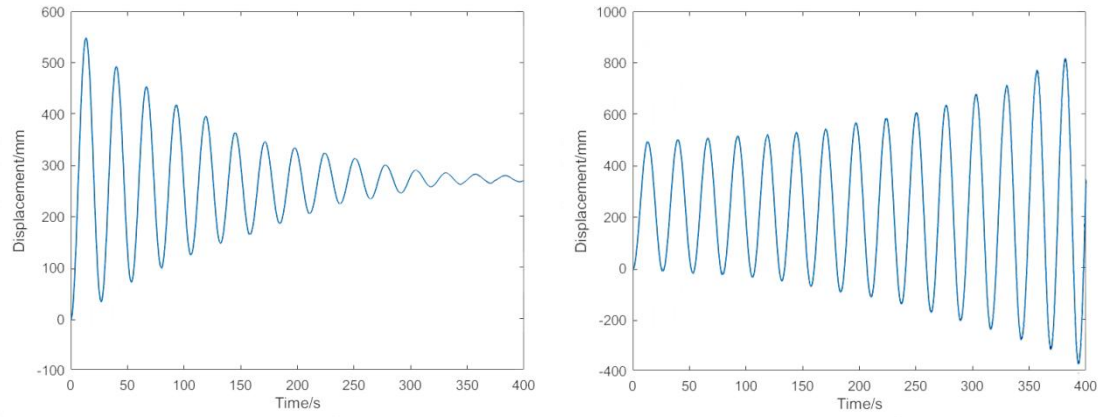

(a) Convergence at 23.80 m/s (b) Divergence at 24.00 m/s

Figure 7 Linear response result

Taking the gap value b as 0.5 mm and the stiffness K_0 outside the free play section as 2000 N/mm, the midpoint of the model wingtip is used as the monitoring point to study the impact of nonlinear aeroelastic response of free play. The simulation results are shown in Figure 8-10, and this paper only captures the stable segment of the time-domain results. It can be seen that compared with the linear time-domain response results, when the speed reaches 21.52 m/s, the model dynamic response gradually enters into a state of constant amplitude oscillation, where the amplitude does not change with time. The phase plot diagram shows a ring shape, and the vibration frequency remains constant, indicating that the system exhibits a limit cycle oscillation (LCO). With the increase of the speed, the system motion maintains constant amplitude oscillation. When the speed reaches 24.00 m/s, the model response diverges, and flutter occurs. Overall, the nonlinearity of free play causes the system to enter a limit cycle oscillation at a lower flutter speed, and the stable limit cycle oscillation can be maintained within a certain speed range, with its amplitude not increasing indefinitely. The divergence speed of the nonlinear system with free play is consistent with the linear analysis results, thus the nonlinearity of free play does not affect the divergence speed.

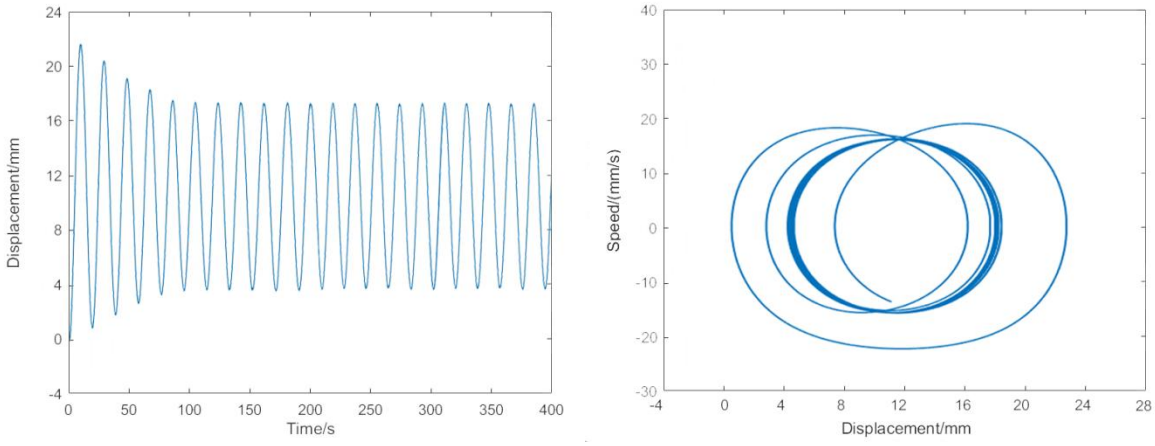

Figure 8 Nonlinear response result and phase plot of speed at 21.52 m/s

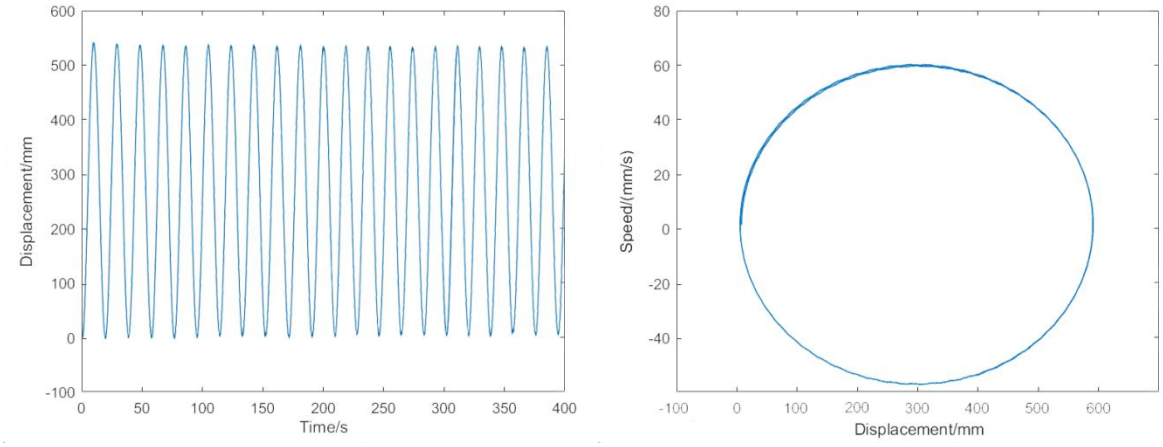

Figure 9 Nonlinear response result and phase plot of speed at 23.80 m/s

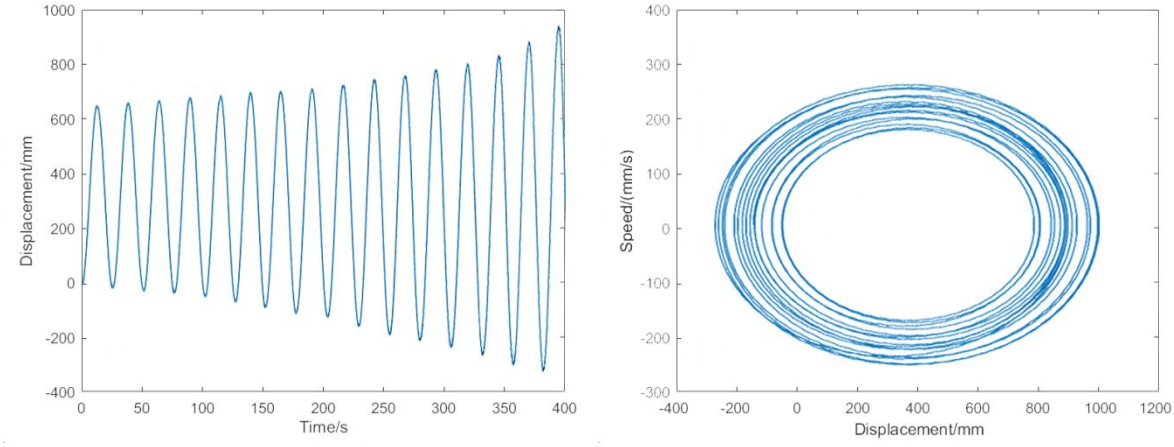

Figure 10 Nonlinear response result and phase plot of speed at 24.00 m/s

3.4 Influence of Nonlinear Parameters of Free Play

3.4.1 Influence of gap value b

The stiffness K_0 outside the free play section is kept constant at 2000 N/mm, and the gap values b are taken as 0.5, 1.0, and 2.0 mm, respectively, to study the influence of the gap value on the limit cycle oscillation of the unmanned MBA. The simulation results are shown in Figure 11. It can be seen that the motion form of the nonlinear system corresponding to different gap values is consistent, the magnitude of the gap value does not affect the entry and divergence speed of the limit cycle oscillations. Within a certain range of limit cycle oscillations (i.e., speed from 21.52 m/s to 24.00 m/s), the greater the speed, the greater the amplitude of the limit cycle oscillations; at the same speed, the larger the gap value, the greater the amplitude of the limit cycle oscillations.

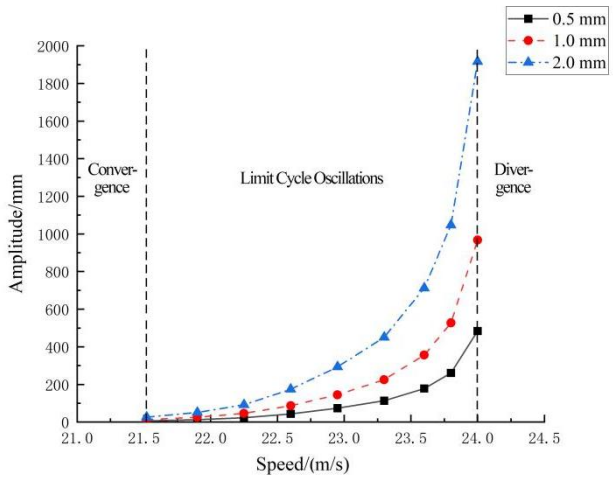

Figure 11 Influence of free play on response amplitude

The variation in amplitude ratios between different gap values is shown in Figure 12, where amplitude ratio 1 is the limit cycle oscillation amplitude ratio between gap values of 1.0 and 0.5 mm, and amplitude ratio 2 is the limit cycle oscillation amplitude ratio between gap values of 2.0 and 0.5 mm. The results indicate that the amplitude ratio is essentially consistent with the gap value ratio; when the gap value is doubled, the limit cycle oscillation amplitude also approximately doubles; under the same speed, the limit cycle oscillation amplitude corresponding to a unit gap value remains essentially unchanged.

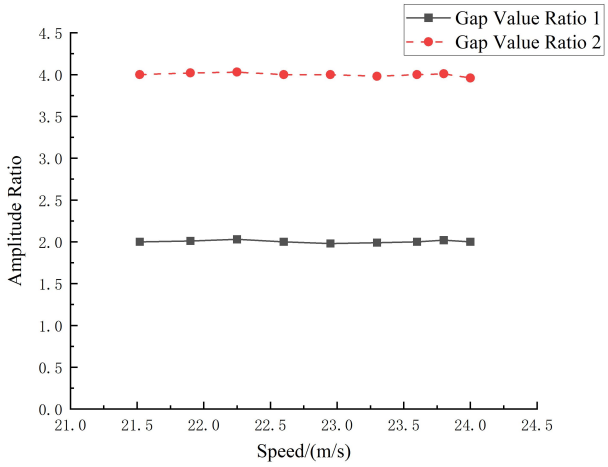

Figure 12 Variation of LCO amplitude ratio with different free play condition

3.4.2 Influences of the stiffness K_0 outside the free play section and the damp coefficient

The gap value b is kept constant at 0.5 mm, and the influences of the stiffness K_0 outside the free play section and the damp coefficient on the characteristics of the limit cycle response are investigated separately.

The stiffness K_0 outside the free play section is analyzed with variable parameters, and the results are shown in Figure 13. The results show that the stiffness K_0 primarily affects the system's divergence speed, while having a smaller impact on the entry speed at which limit cycle oscillations occur; the larger the stiffness K_0, the greater the system's divergence speed, and the wider the velocity range where the system exhibits limit cycle oscillations.

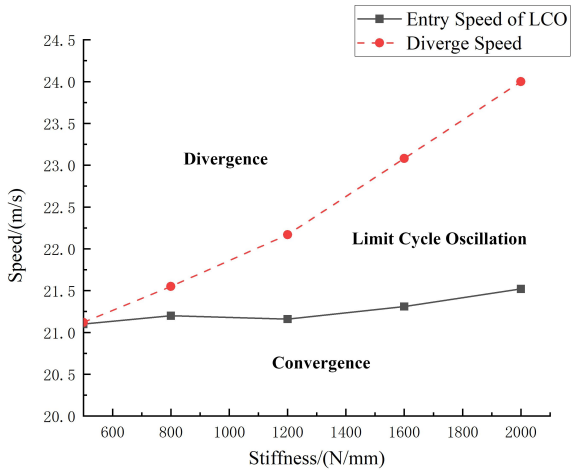

Figure 13 Influence of K_0 on LCO

The value of the stiffness K_0 outside the free play section is kept constant at 2000 N/mm, and the damp coefficients are taken as 0.01, 0.02, and 0.03, respectively, and the results of the variable parameters are shown in Figure 14.

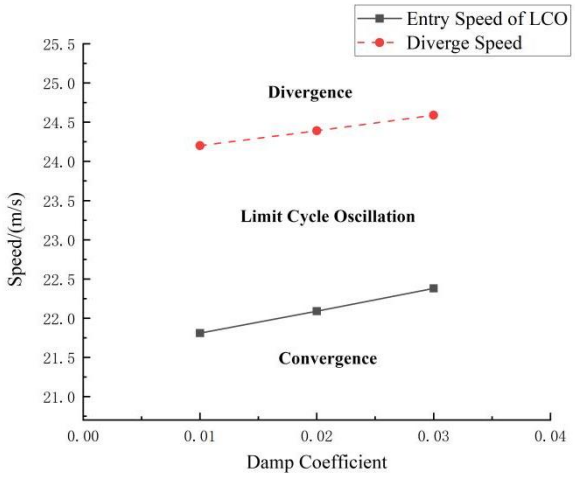

Figure 14 Influence of damp coefficient on LCO

It can be seen from Figure 14 that the damp coefficient mainly affects the critical divergence speed of the system, the larger the damp coefficient, the greater the critical divergence speed of the system and the critical speed for entering limit cycle oscillations, but overall it essentially does not affect the width of the system's limit cycle oscillation velocity range.

4 CONCLUSION

(1) A finite element model is established for the two-aircraft combined unmanned multi-body aircraft with wingtip hinge connections, and the nonlinear system is modeled based on the fictitious mass method by applying fictitious mass at the structural free play to generate modal shape with fictitious mass. Using this method with consideration of the effect of nonlinear stiffness, modal analysis and aeroelastic response analysis are conducted for both the linear and nonlinear models, taking into account the effects of nonlinear stiffness, and these can meet the basic requirements of engineering design. In the process of parameter study, when the stiffness changes, only one modal analysis is needed, and there is no need to do the modeling and modal analysis again for the new structure, which saves the time of modal analysis and effectively improves the efficiency of the aeroelastic response analysis.

(2) By conducting a nonlinear aeroelastic analysis on the two-aircraft combined unmanned multi-body aircraft, when there is a free play exists in the docking area of the wingtip, a nonlinear oscillation phenomenon named limit cycle oscillation (LCO) will occur on the wing surface within a specific velocity range below the linear flutter boundary.

(3) The magnitude of the gap value b only affects the amplitude of the limit cycle oscillations, without affecting the critical speed of the limit cycle oscillations. Under the same speed, the larger the gap value b is, the greater the amplitude of the limit cycle oscillations is. The stiffness value K_0 outside the free play section affects the divergence speed of the limit cycle oscillations. The larger the stiffness value K_0, the greater the divergence speed of the system, and the wider the velocity range where the system exhibits limit cycle oscillations. The damp coefficient causes a shift in the speed region of limit cycle oscillations, but overall, it does not significantly affect the width of the system's limit cycle oscillation velocity range.

This work was supported by the National Natural Science Foundation of China (Grant No. 12202442)

REFERENCES

[1] Knoedler A J. Lowering the high ground using near-space vehicles for persistent ISR[J]. *Military Technology*, 2008, *32(6)*, 178.

[2] Moomey E R. Technical Feasibility of Loitering Lighter-than-air-Near-space Maneuvering Vehicles[J]. 2005.

[3] Love M, Zink P, Wieselmann P, et al. Body freedom flutter of high aspect ratio flying wings[C]//*46th AIAA/ASME/ASCE/AHS/ASC Structures, Structural Dynamics and Materials Conference*, 2005: 1947.

[4] Wang X, Van Kampen E, Chu Q P, et al. Flexible aircraft gust load alleviation with incremental nonlinear dynamic inversion[J]. *Journal of Guidance, Control, and Dynamics*, 2019, *42(7)*: 1519-1536.

[5] Wright-Patterson A F B. United states air force museum guidebook[M]. *Ohio: Air Force Museum Foundation*, 1975.

[6] Anderson C E B. Dangerous experiments: Wingtip coupling at 15000 feet[J]. *Flight Journal*, 2000, *5(6)*: 64.

[7] Miller J. Project Tom-Tom[J]. *Aerophile*, 1975, *1(3)*: 1-9.

[8] Magill S A. Compound aircraft transport study: Wingtip-docking compared to formation flight[D]. Virginia Polytechnic Institute and State University, 2002.

[9] Wlach S, Balmer G, Hermann M, et al. Elaha–Elastic Aircraft for High Altitudes[C]. 23rd ESA Symposium on European Rocket and Balloon Programmes and Related Research. Noordwijk : ESA, 2017: 1-5.

[10] Montalvo C, Costello M. Meta aircraft connection dynamics[C]//*AIAA Guidance, Navigation, and Control Conference*, 2012: 4677.

[11] Montalvo C, Costello M. Meta aircraft flight dynamics[J]. *Journal of Aircraft*, 2015, *52(1):* 107-115.

[12] Troub B, Montalvo C J. Meta aircraft controllability[C]//*AIAA Atmospheric Flight Mechanics Conference*, 2016: 3395.

[13] Meng Y, Chao A, Xie C C, et al. Conceptual design and flight test of two wingtip docked multi-body aircraft[J]. *Chinese Journal of Aeronautics*, 2022, *35(12)*: 12.

[14] Behrens A, Grund T, Ebert C, et al. Investigation of the aerodynamic interaction between two wings in a parallel flight with close lateral proximity[J]. *CEAS Aeronautical Journal*, 2020, *11*: 553-563.

[15] Alexander K, Alexander B, Alexander H, et al. Closed-loop flight tests with an unmanned experimental multi-body aircraft[C]//*17th international forum on aeroelasticity and structural dynamics*, Como, Italy. 2017.

[16] CHEN S, LI Q Y, RAN Y G. Research on the vibration characteristics of an all-movable wing with two dimensional freeplay nonlinearity[J]. Journal of Sichuan University of Science & Engineering(Natural Science Edition), 2017, *30(1)*: 60-64.

[17] CHEN S, LI Q Y, TAN G H. Influence of control surface with freeplay nonlinearity on flutter characteristics[J]. *Applied Mathematics and Mechanics*, 2014, *35(s1)*: 90-94.

[18] LI Z T, HAN J L, YUAN H W. Simulation and tests for aeroelasticity of a fully moving rudder surface with bilinear nonlinearity[J]. *Journal of Vibration and Shock*, 2020, *39(19)*: 234-242.

[19] QIAN W, BAI Y G, CHEN X Y, et al. Aeroservoelastic analysis of a hypersonic aircraft[J]. *Journal of Low Frequency Noise Vibration and Active Control*, 2018, *37(3)*: 534-553.

[20] HUANG C D, ZHENG G N, YANG G W, et al. Aeroelastic study of a three dimensional all-movable wing with free play using CFD/CSD coupling[J]. *Chinese Journal of Applied Mechanics*, 2018, *35(1)*: 1-8.

[21] NI Y G, HOU C, WAN X P, et al. Aeroelastic analysis of a folding wing with structural nonlinearities[J]. *Journal of Vibration and Shock*, 2016, *35(18)*: 165-171.

[22] WANG F, RAN Y G, TAN G H, et al. Nonlinear aeroelastic response analysis of fully moving wing with free play[J]. *Advances in Aeronautical Science and Engineering*, 2022, *13(2)*: 18-26.

[23] ZHANG W W, WANG Z B, YE Z Y, et al. Effect of angle of attack on flutter characteristics of a control surface with free-play nonlinearity[J]. *Journal of Mechanical Strength*, 2011, *33(2)*: 296-301.

[24] LEE B H K, LIU L, CHUNG K W. Airfoil motion in subsonic flow with strong cubic nonlinear restoring forces[J]. *Journal of Sound and Vibration*, 2005, *281(3)*: 699-717.

[25] YANG N, WANG N, ZHANG X, et al. Nonlinear flutter wind tunnel test and numerical analysis of folding fins with freeplay nonlinearities[J]. *Chinese Journal of Aeronautics*, 2016, *29(1)*: 144-159.

[26] LI J X, TIAN W, GU Y S. Nonlinear aeroelastic analysis of control fin with free-play nonlinearity[J]. *Advances Aeronautical Science and Engineering*, 2020, *11(6)*: 827-836.

[27] ZHANG F, CHENG F. Nonlinear flutter analysis of certain airplane with freeplay[J]. *Advances Aeronautical Science and Engineering*, 2021, *12(4)*: 99-104.

[28] KARPEL M, RAVEH D. Fictitious mass element in structural dynamics[J]. *AIAA Journal*, 1996, *34(3)*: 607-613.

[29] KARPEL M, MOULIN B. Aeroelastic loads in response to concentrated excitation using fictitious masses[C]// *Proceeding of 46th AIAA/ASME/ASCE/AHS/ASC Structures, Structural Dynamics, and Materials Conference*. Austin, Texas: AIAA, 2005: 2371-2381.

COPYRIGHT STATEMENT